



HAL
open science

Formation of annealing twins during primary recrystallization of two low stacking fault energy Ni-based alloys

W Wang, S Lartigue-Korinek, F Brisset, A L Helbert, J Bourgon, T Baudin

► **To cite this version:**

W Wang, S Lartigue-Korinek, F Brisset, A L Helbert, J Bourgon, et al.. Formation of annealing twins during primary recrystallization of two low stacking fault energy Ni-based alloys. *Journal of Materials Science*, 2015. hal-03301329

HAL Id: hal-03301329

<https://hal.science/hal-03301329>

Submitted on 27 Jul 2021

HAL is a multi-disciplinary open access archive for the deposit and dissemination of scientific research documents, whether they are published or not. The documents may come from teaching and research institutions in France or abroad, or from public or private research centers.

L'archive ouverte pluridisciplinaire **HAL**, est destinée au dépôt et à la diffusion de documents scientifiques de niveau recherche, publiés ou non, émanant des établissements d'enseignement et de recherche français ou étrangers, des laboratoires publics ou privés.

Formation of annealing twins during primary recrystallization of two low stacking fault energy Ni-based alloys

W. Wang^{1*}, S. Lartigue-Korinek^{2a}, F. Brisset^{1b}, A. L. Helbert^{1c}, J. Bourgon^{2d}, T. Baudin^{1e}

¹Université Paris-Sud, ICMMO, UMR CNRS 8182, 91405 Orsay Cedex, France

²Institut de Chimie et des Matériaux Paris Est, MCMC, UMR CNRS 7182, 94320 Thiais, France

Corresponding Author: wei.wang@u-psud.fr, Université Paris-Sud, ICMMO, UMR CNRS 8182, bât. 410, 91405 Orsay Cedex, France. Tel: + (33) 1 69 15 47 89, Fax: + (33) 1 69 15 47 97.

a lartigue@icmpe.cnrs.fr

d bourgon@icmpe.cnrs.fr

b francois.brisset@u-psud.fr

e thierry.baudin@u-psud.fr

c anne-laure.helbert@u-psud.fr

Abstract.

First stages of recrystallization are analyzed in low stacking fault energy nickel alloys cold rolled and subsequently annealed at 700°C for 6 minutes. These alloys are envisaged as candidate materials for the heat exchanger of VHTR (Very High Temperature Reactor) that works at 1000°C. First recrystallized grains show evidence of extensive twinning that is studied by Transmission Electron Microscopy. Specific twinning features such as five-fold twin and microtwins bordered by partial dislocations are revealed. Twin density increases with increasing amounts of prior deformation before annealing. The local crystal orientations are determined at a nanometer scale. It is shown directly that when twinning occurs, the recrystallized area beyond the twin has a lower stored deformation energy. Thus recrystallization and the associate twinning induce a decrease in the total stored deformation energy.

Keywords: Nickel alloy, Twinning, Stored energy, TEM, EBSD

1 Introduction

Ni based alloys with low stacking fault energy (SFE) display extensive twinning from the start of primary recrystallization. Twinning occurs in recrystallized grains behind migrating grain boundaries (GBs). Until now, most studies concerned the mechanisms of twinning during grain growth. But, very few is known on the occurrence of twinning at the very beginning of primary recrystallization. The main driving forces for GB migration are supposed to be different during primary

recrystallization and grain growth, however twinning events are related in both cases to GB migration and require a driving force. Twins are connected to migrating GBs and the mechanism of twinning could be similar. With respect to the formation of twinning during grain growth, Fullman and Fisher in 1951 [1] proposed that twins are formed near triple junctions of moving grain boundaries, the driving force being an overall decrease in interfacial energy. Twinning was then explained by a stacking error or a 'growth accident' occurring at

1 GBs or triple junctions that induces the
2 splitting and subsequent migration of a GB
3 segment, leaving behind two coherent twin
4 boundaries [2]. Following this approach,
5 Gleiter [3] proposed an atomistic model that
6 involves a two dimensional nucleation on
7 close packed planes of the growing grain
8 just at the point where the GB is parallel to
9 $\{111\}$ planes of the growing grain. A quite
10 different nucleation process was also
11 proposed which involves a direct stacking
12 fault emission at GB ledges producing two
13 twin segments, a coherent twin and an
14 incoherent one; the further migration of the
15 incoherent twin may induce a twinned
16 region [4]. In all these works, the driving
17 force is a reduction in the overall interfacial
18 energy. If recovery is not completed, a
19 decrease in dislocation density is also
20 evoked [4]. But, a limitation of these models
21 is that the initial orientation relationship
22 between two grains must be close to a twin
23 orientation, or the newly formed GB must
24 have a low energy, two conditions that seem
25 difficult to realize. Both experiments and
26 simulation find that most GBs have a high
27 interfacial energy [5-6].

28 In an attempt to interpret all the
29 features of annealing twins, a microscopic
30 model proposes that annealing twins are
31 produced with the formation of a partial
32 Shockley loop at the $\{111\}$ ledges formed in
33 migrating GBs [7-8]. The theory is based on
34 the idea that annealing and deformation
35 twins are crystallographically identical. The
36 higher the GB velocity, the higher the
37 probability for twin nucleation. Twin
38 emission by migrating GBs during
39 recrystallization had been evidenced
40 previously, the twin nucleus being a stacking
41 fault or a thin packet of stacking faults,
42 bordered by Shockley partial dislocations
43 [9]. The tips of annealing twins could be
44 described as arrays of Shockley partial

dislocations, but were fundamentally
different from deformation twins in that for
the tips of annealing twins the partials can
be equally distributed amongst all three
partials, allowing for a blocky tip and strain
relaxation since the net burgers vector can
cancel.

The emission of partial dislocations has
also been found by Molecular Dynamics
(MD) to interpret twinning during grain
growth in nanocrystalline copper [10].
However in the recent experiments on twin
characteristics in nanocrystalline thin films,
the authors exclude such a mechanism,
arguing that the required internal stresses are
too high [11].

In recrystallized materials that have
undergone a high deformation level before
annealing, some twin characteristics are
worth noticing. From a mesoscopic point of
view it was found in nickel that the density
of annealing twins decreases with the grain
size, whatever time and temperature, and
depends on the driving force for GB
migration [12]. The twin number/grain size
dependence applied well with other low SFE
materials such as copper alloys [12]. The
weak dependence of twinning with
temperature is consistent with the model
based on dislocation emission [7]. In the
particular case of low temperature annealing
where recovery is predominant, twinning
started when the grain growth or GB
migration was restrained, as revealed in
copper and nickel by in situ experiments
[13-14]. Thus twinning is tightly linked to the
further onset of grain boundary migration.
The studies during early stage of
recrystallization revealed also that twinning
promotes the nucleation process in two types
of stainless steel and α -brass [15].

The occurrence of twinning during
recrystallization and especially the role of
the deformation level prior to the heat

1 treatment is worth studying as it could shed 43
2 light on twinning phenomena, in particular 44
3 the relationship between onset of twinning 45
4 and stored energy. Our previous works on 46
5 recrystallization in nickel alloys have shown 47
6 that the number of $\Sigma 3$ GBs increased with 48
7 the stored energy resulting from a prior 49
8 deformation before annealing [16]. A similar 50
9 result was found in an austenitic stainless 51
10 steel [17]. Moreover, the twin density 52
11 increases during recrystallization and 53
12 decreases during grain growth in pure nickel 54
13 and twin formation was only observed for 55
14 GBs migrating into deformed regions [18]. 56

15 The present paper analyzes the twin 57
16 formation in two nickel-based alloys by 58
17 putting the focus on the features occurring in 59
18 the very first stages of recrystallization. 60
19 These materials have much lower stacking 61
20 fault energy γ_{SFE} (between 4 and 10 mJ/m²) 62
21 than pure nickel and copper alloys. 63
22 Twinning features are investigated by 64
23 Transmission Electron Microscopy (TEM). 65
24 The originality of this study is to determine 66
25 the local orientations at a nanometer scale, 67
26 allowing establishing a relationship between 68
27 twinning and intragranular stored energy. 69
28 Twinning mechanisms during first stages of 70
29 recrystallization are finally discussed. 71

31 2 Experimental details

32 Two nickel alloys were produced by 74
33 hot forging. One is monophasic (sample A), 75
34 the other contains W particles as a second 76
35 phase (sample B). Their chemical 77
36 compositions are presented in table 1. For 78
37 both materials, sheets of 1 cm thickness 79
38 were cut from the ingots, cold-rolled with 90% 80
39 reduction and annealed at 900°C for 3 hours 81
40 in argon atmosphere. Under these treatments, 82
41 a homogenous distribution of the chemical 83
42 composition was obtained, together with a

homogenous microstructure and an almost
isotropic texture. The mean grain size is
about 17 μm for sample A and 8 μm for
sample B in these conditions. Afterwards,
the sheets were cold-rolled with different
reduction level and the corresponding true
strains are shown in table 2. Then they were
annealed at 900°C during 4 min so as to
obtain a complete recrystallization [16].
Moreover, for each material, the one
deformed with 80% reduction was annealed
during 6 min at 700°C so as to develop the
first stage of recrystallization.

The microstructure after annealing was
studied on the transverse plane (Rolling
Direction RD - Normal Direction ND) with
a TSL/EDAX Electron BackScatter
Diffraction (EBSD) system installed on a
Field Emission Gun Scanning Electron
Microscope (FEG-SEM). The analyzed
maps were based on hexagonal grid. Those
after complete recrystallization (900°C)
were analyzed for an area of 150 x 350 μm^2
with 100 nm as step size, and the densities
of $\Sigma 3$ and $\Sigma 9$ GBs were analyzed statistically.
Those after partial recrystallization (700°C)
were studied with 50 nm as step size. All
samples were prepared by mechanical
polishing up to 1/4 μm diamond polishing
and finally polished using a colloidal silica
suspension (OPS) with particle size of about
0.04 micron.

In the samples that underwent first
stage of recrystallization, the recrystallized
areas were studied with a JEOL 2000EX
TEM. Thin foil preparation is described in
[19]. The distribution of misorientations was
determined thanks to an Automatic Crystal
Orientation Mapping (ACOM) system in a
FEI Tecnai F20 TEM (spot size 8, camera
length 7.1 cm, condenser aperture 10 μm ,

Table 1 chemical composition of the studied nickel alloys

Wt.%	Ni	Cr	W	Si	Mn	Mo	Al	Ti
Sample A	68.8	5.7	25.2	0.065	0.086	0.07	0.08	0.13
Sample B	60.7	19.6	19.9	0.075	0.08	0.05	0.1	0.14

1 gun lens 6, extraction voltage at 4.3 kV, 36
 2 resulting probe size 1.2 nm). An ASTAR
 3 system was used for ACOM diffraction data 37
 4 acquisition [20]. The analyzed map step was 38
 5 10 nm based on a square grid. The 39
 6 crystallographic orientations are obtained 40
 7 through image matching between the 41
 8 experimental diffraction pattern and 42
 9 calculated templates with an orientation step 43
 10 of one degree between two successive 44
 11 templates.

Table 2 True strain prior to annealing

Rolling reduction	40%	60%	80%
True strain	0.59	1.06	1.86

14
 15 EBSD and ACOM data were processed 52
 16 by using the OIM™ software. For each 53
 17 point of scanned area, the retained images 54
 18 describe an Image Quality (IQ) that depends 55
 19 on the distortion of crystal lattice. This 56
 20 parameter is useful for the embodiment of 57
 21 the strain distribution in the material. 58
 22 Moreover, for each pixel, the Inverse Pole 59
 23 Figure (IPF) shows the crystal direction that 60
 24 is aligned with the chosen direction of 61
 25 reference (IPF [100], [010] and [001] mean 62
 26 respectively the rolling direction, the 63
 27 transverse direction and the normal direction 64
 28 of sample that is the reference direction). 65
 29 Then the pixels are colored according to the 66
 30 code defined in the unit triangle (for 67
 31 example, the red color in IPF [001] means 68
 32 the crystal direction <001> of the pixel is 69
 33 parallel to the normal direction of the 70
 34 sample).

35

3 Results

3.1 Recrystallization mechanisms

Fig. 1 shows the microstructure of two materials after a 6 min annealing at 700°C. New grains can be found within the surrounding deformed environment. The recrystallization seems to be faster in sample B than in A, with upper number of new grains. A statistical study with the help of microharness analyses shows that the recrystallization fraction is 6% and 8% in sample A and B respectively. The formation of $\Sigma 3$ GBs was observed inside these new grains for both materials. The little recrystallization advantage in sample B should be related to the presence of second phase. Indeed, during the cold deformation, second phase particles act as obstacles to dislocation slip. This induces the formation of local deformation around particles, which become favorable sites for nucleation of recrystallized grains during subsequent annealing. This recrystallization mechanism is called particle stimulated nucleation (PSN) [21].

Figs. 2a-b show the presence of a bulge in sample A after the same annealing process. The crystal close to the bulge may be seen as a small recrystallized grain which could have been produced according to the Strain Induced Boundary Migration (SIBM) mechanism. This mechanism, firstly observed in 1950 [22], is related to the migration of a pre-existing grain boundary, leaving a dislocation free area behind it [21]. A similar microstructural feature occurs in a Fe-36%Ni alloy [23]. Such a bulge is also proposed to occur by the stress-driven GB

1 motion during the deformation [24]. In any 3 very small which favors its growth towards
 2 case the stored energy behind the bulge is 4 the adjacent area with a higher stored energy.

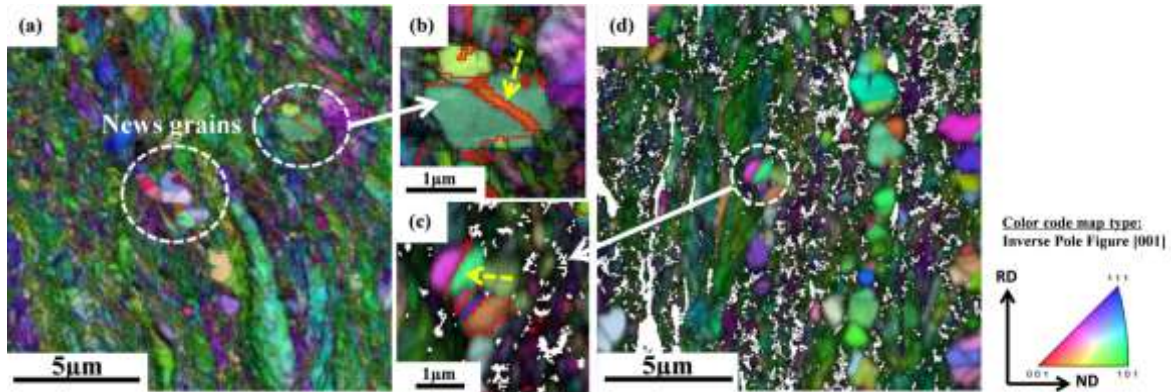


Fig. 1 Images issued from EBSD analyses (FEG-SEM) showing IQ + IPF [001] map (a) sample A. Regions with new recrystallized grains are circled. One of them is enlarged in (b); (c) and (d) sample B after annealing at 700°C for 6 min. GBs in red correspond to $\Sigma 3$ (yellow arrow). The white areas in (c) and (d) are the clusters of second phase W

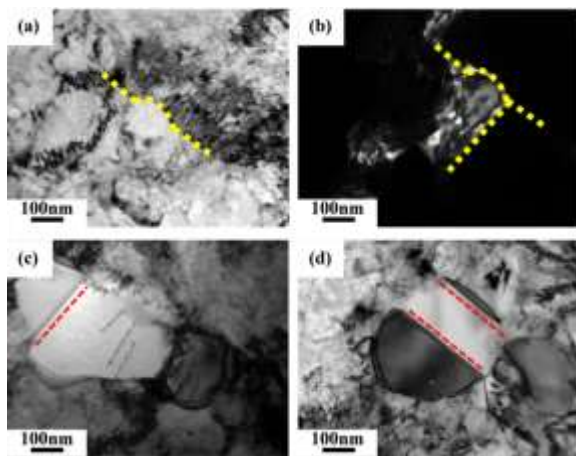


Fig. 2 TEM images after annealing at 700°C for 6 min of sample A. (a) bright-field image and (b) dark-field image indicating bulging of a GB; (c) and (d) bright-field images showing formation of twins inside the new grains during recrystallization. The red and yellow lines show the $\Sigma 3$ and the pre-existing grain boundaries, respectively

11 Figs. 2c-d reveal the presence of annealing twins inside new grains. Some isolated dislocations lie within the grain and are parallel to the twin boundaries. The twin boundary traces are thus aligned with one of the {111} planes (slip dislocation planes) of

17 the recrystallized grains. This reveals that
 18 coherent twins are formed at the very
 19 beginning of the primary recrystallization. A
 20 microtwin parallel to a {111} plane presents
 21 dislocations at its extremity (Fig. 3a). In the
 22 2 beam conditions of fig. 3b, the twin is not
 23 visible and the dislocations show a
 24 symmetrical contrast characteristic of $g \cdot b = 0$,
 25 in agreement with a Burgers vector of
 26 twinning dislocations equal to $1/6 [2-1-1]$.

27 The local microstructure of sample B
 after annealing is shown in figure 4. The
 28 new grains are either close to or distant from
 29 the W particles (Fig. 4a). SIBM and PSN
 30 mechanism have been both activated. The
 31 simultaneous presence of two
 32 recrystallization mechanisms can explain the
 33 little advantage of recrystallization at the
 34 beginning of annealing in sample B.

35 Multiple twinning occurs within new
 36 grains. (Figs. 4b-d). As many twins are
 37 formed from the same parent grain adjacent
 38 twins can meet each other and form $\Sigma 9$
 39 boundary at the triple junction (yellow line
 40 in Fig. 4c). This phenomenon has been
 41 largely studied during grain boundary

1 engineering, where a large number of Σ_3 3 dissociation of GBs [25].
 2 ($n \geq 1$) GBs is related to the association and

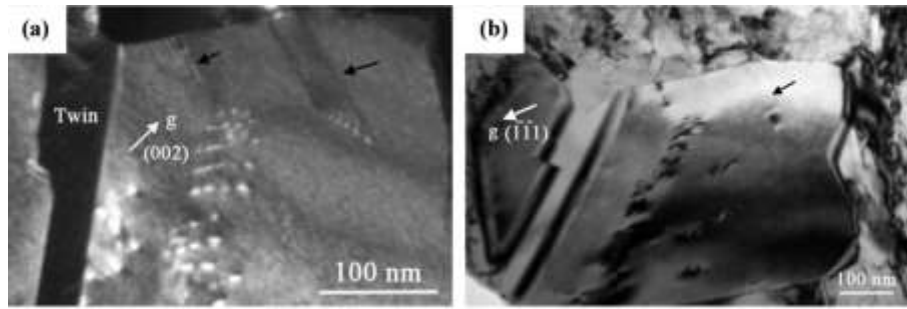


Fig. 3 TEM images after annealing at 700°C for 6 min of sample A. (a) Dark field image (2-beams conditions $g=(002)$) showing a twin and two microtwins (arrowed) inside a recrystallized grain. On the bright field image (b), the arrowed microtwin is out of contrast, but the dislocations at its extremity show a symmetrical contrast

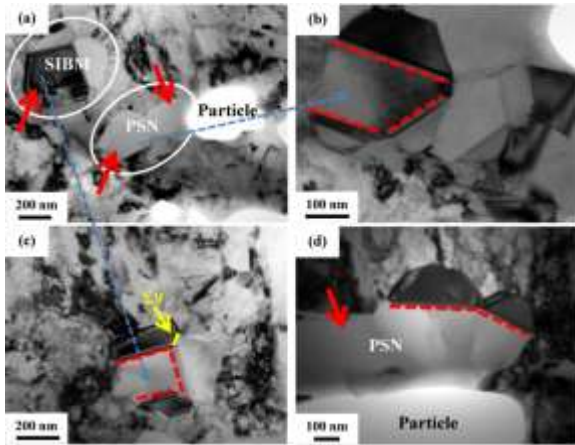


Fig. 4 Bright field TEM images of sample B after annealing at 700°C for 6 min. (a) Bright-field image showing recrystallized areas associated with SIBM and PSN. The particles have been dissolved during thinning; (b)-(d) multiple twins occur inside new grains. The red and yellow lines show the Σ_3 and Σ_9 boundaries, respectively

3.2 Annealing twin

The Figs. 5 and 6 show ACOM maps for samples A and B, respectively. The red lines are the GBs which have the Σ_3 misorientation relationship. In Fig. 5c, the blue lines show the 4 $\{111\}$ crystal plane traces on each side of the Σ_3 boundary and the dotted ones show the common plane.

19 The mean trend line of Σ_3 is shown with
 20 orange dotted line. Thus the Σ_3 boundary is
 21 parallel to a common $\{111\}$ plane and
 22 corresponds to a coherent one, as most twins
 23 indicated by red lines in the recrystallized
 24 grains of Figs. 5a and 6a. This type of twin
 25 boundaries is always straight.

26 In addition, incoherent twin boundaries
 27 Σ_3 incoh are also present and an example is
 28 indicated with yellow line (boundary 2) in
 29 Fig. 5d. This twin part is located between
 the boundaries 1 and 3 that are coherent
 twins. The formation of this incoherent twin
 should be the outcome of the different
 formation times and/or locations of the two
 coherent twins. A similar feature is found by
 MD simulations [10].

The incoherent twin boundary is
 conventionally defined by its plane that is
 close to a common $\{112\}$ plane. This
 definition is then extended to all boundaries
 whose plane is different from a common
 $\{111\}$ plane [25]. In Fig. 5d, the Σ_3 incoh
 boundary 2 is deviated from the $\{112\}$ and
 $\{111\}$ orientations. However, it could be
 faceted at the atomic level.

The grain in the center of Fig. 5a shows
 evidence of five-fold twinning. This feature

1 is rather surprising as it usually occurs in 9 perfect CFC lattice is 70.53° , a disclination
 2 nanoparticles or nanocrystalline materials.10 with an angle close to 7.5° must occur. Such
 3 Observed for the first time in 1959 [26],11 a defect is usually accommodated elastically
 4 five-fold twins are described as five crystals12 or with the formation of sub-boundaries
 5 twin-related to each other, the five twin13 [27-28]. In the present case, a sub-boundary
 6 planes sharing a common $\langle 110 \rangle$ direction.14 is present close to a twin and starts from the
 7 The apex angle between twins should be 72° 15 center of the five-fold twin as shown in Fig.
 8 $(360^\circ/5)$. As the angle between twins in a16 5b.

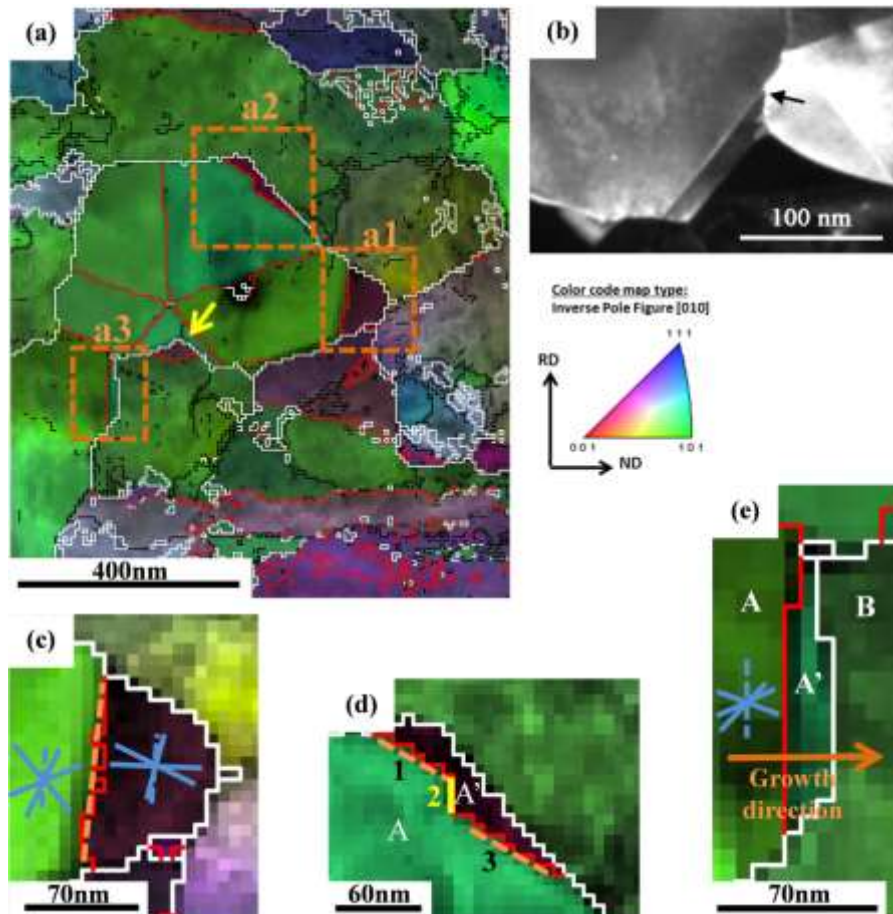


Fig. 5 Maps of grain orientations obtained by TEM with the ACOM system (IQ+IPF, color code for an inverse pole figure [010]), for sample A after annealing at 700°C for 6 min. (a) Several grains show the presence of twins. A five-fold twin occurs in the central grain. (b) Bright field image of the five-fold twin showing the sub-boundary (white arrow), indicated by a yellow arrow in Fig. 5a. The three regions delimited by squares a1, a2 and a3 are enlarged in (c) (d) and (e) respectively. Red lines figure $\Sigma 3$ GBs, white lines High Angle GBs other than twins and black lines Low Angle GBs (LAGBs). The blue lines show the traces of 4 $\{111\}$ plane traces in each grain. The blue dotted lines show the trace of the common twin plane on each side of the twin, and the orange arrow shows the growth direction deduced from the curvature of the migrating boundary. The yellow arrow indicates the presence of a sub-grain in the five-fold twin

1 The mechanisms proposed for
2 formation of five-fold twins as reviewed in
3 [29] distinguish cyclic twinning operation
4 due to either a mistacking of atoms or
5 deformation twinning as an accommodation
6 process of plane strains in growing thin
7 films [29]. However the mechanism of
8 five-fold growth in polycrystalline
9 nanosized metals has not been evidenced
10 experimentally. MD simulations of grain
11 growth in nanocrystalline copper at zero
12 external pressure, and high temperature
13 reveal that five-fold twins occur during
14 annealing [30]. Five-fold twins result from
15 local shear stresses at GBs and the proposed
16 mechanism is a sequential emission of
17 partial dislocations as reported in [31]. This
18 work demonstrates that very high stresses
19 are present and originate from the small
20 grain size in the absence of any applied
21 stress.

22 3.3 Influence of deformation on 23 annealing twins

24 The influence of deformation on
25 annealing twin formation was investigated
26 after complete recrystallization at 900°C on
27 samples that underwent increasing levels of
28 deformation. The recrystallization was
29 finished after 4 min thus the recovery
30 process was considered to be negligible
31 [16].

32 The densities of $\Sigma 3$ (including $\Sigma 3_{\text{coh}}$
33 and $\Sigma 3_{\text{incoh}}$), and $\Sigma 9$ GBs were analyzed in
34 these completely recrystallized samples. For
35 each GB type, the density is defined as its
36 total length divided by the analysis surface
37 [16, 32]. The total lengths of $\Sigma 3$, $\Sigma 3_{\text{coh}}$ and
38 $\Sigma 9$ obtained from OIMTM analysis are shown
39 in Fig. 6 as a function of deformation prior
40 to the annealing. The $\Sigma 3_{\text{coh}}$ density
41 increases with increasing deformation,
42 except for the sample B after stronger
43 deformation ($\epsilon=1.86$). This exception is

interpreted by the very small average grain
size after complete recrystallization (grain
size = 2.2 μm). The length of some $\Sigma 3_{\text{coh}}$
boundary is very short; it does not contain
enough pixels by segment, and can be hardly
recognized as $\Sigma 3_{\text{coh}}$ by OIMTM analysis
[33]. However, with regard to the density of
total $\Sigma 3$ GBs, it always increases with
increasing deformation. All these results
indicate that a higher stored energy before
recrystallization favors the formation of twin
boundaries.

Besides, the $\Sigma 3_{\text{incoh}}$ and $\Sigma 9$ GBs are
an outcome from $\Sigma 3_{\text{coh}}$ formation. The
density of $\Sigma 3_{\text{incoh}}$ GBs therefore increases
with deformation. However, the $\Sigma 9$ GB
density is almost identical whatever the
deformation; as it is very low, a possible
small evolution versus the deformation is
difficult to detect.

The stored energy has also an influence
on the velocity of GB migration during
recrystallization. Therefore, the twin
formation may be related to the velocity of
GB migration. One can also find the
densities of these GBs are always greater in
sample B than in A. It is mentioned above
that a local deformation is formed around
the particles. During the subsequent
annealing, this local deformation contributes
to increase locally the GB migration velocity
that favors the twin formation. Such an
effect has already been found in another
Ni-based alloy [32].

4 Discussion

4.1 Active twinning system

In Fig. 5e, the blue lines in the grain A
show the 4 {111} plane traces and it can be
found that the coherent twin AA' matches
one of these planes (dotted one) whose
normal direction is close to the growth
direction. This direction is deduced from the

1 curvature of the migrating boundary. So the 9 grows simultaneously towards two different
 2 formation of coherent twins depends on the 10 directions (respectively indicated by orange
 3 growth direction as already proposed by 11 arrows in area a1 and a2). The coherent
 4 Gleiter [3] and this can explain the 12 twins are perpendicular to the growth
 5 formation of parallel twins in some 13 direction. This feature occurs in both
 6 recrystallized grains like those shown in Fig. 14 materials whatever the involved mechanism
 7 2d. 15 (SIBM and PSN).
 8 In Fig. 7, the new grain formed by PSN

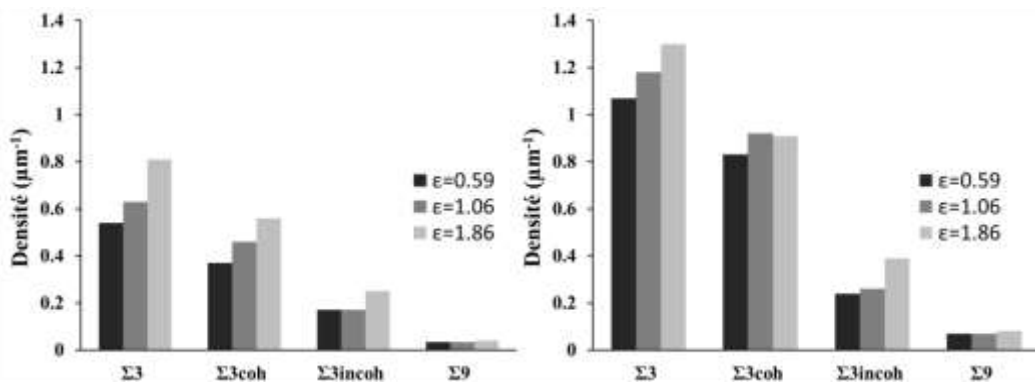


Fig. 6 Densities of $\Sigma 3$ (including $\Sigma 3\text{coh}$ and $\Sigma 3\text{incoh}$), $\Sigma 3\text{coh}$, $\Sigma 3\text{incoh}$ and $\Sigma 9$ GBs after different strain amount followed by the complete recrystallization, respectively for (a) sample A et (b) sample B

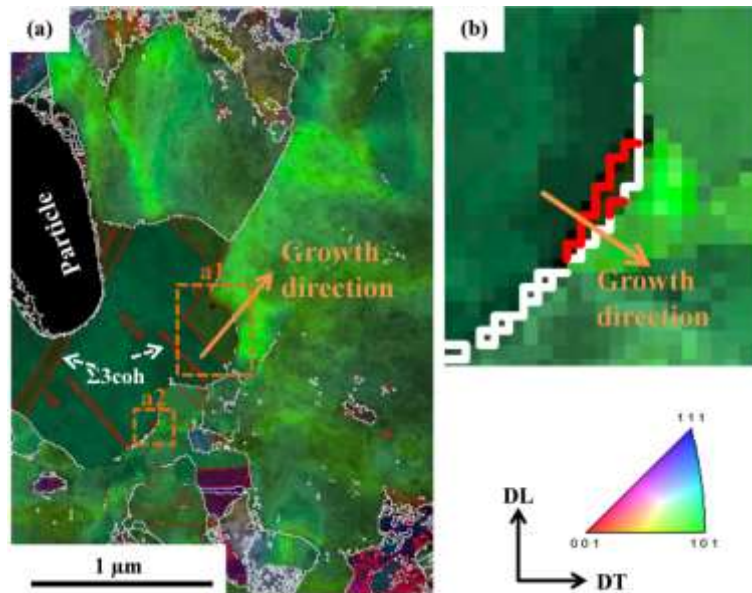


Fig. 7 Maps of grain orientations obtained by TEM with the ACOM system (IQ+IPF, color code for an inverse pole figure [010]), for sample B after annealing at 700°C for 6 min. (a) a new grain close to a W particle display several twins. The area a2 is enlarged in (b). Red and white lines show $\Sigma 3$ GBs and High Angle GBs (HAGBs) respectively. The orange arrow shows the growth direction deduced from the curvature of the migrating boundary

4.2 Energy variation during twin formation

The stored energy of the different grains including twinned grains has been estimated from the determination of local misorientations, using the Kernel Average Misorientation (KAM) calculation [34-35].

The KAM map points out the local misorientation (Fig. 8). The pixel of the ACOM image is coming from a square grid, and the kernel size is chosen considering the 3rd neighboring pixels (or 30 nm). If the misorientation of any 3rd neighboring pixel with respect to the considered pixel is larger than 15°, this pixel will be considered as belonging to another crystal. Every pixel is then color coded as function of its KAM value and twins are indicated by white arrows. The average KAM and standard deviation (StD) for some grains and twinned parts of Fig. 8 are shown in table 3. The misorientation values are small, due to the small kernel size. For some grains, a high StD value reflects an heterogeneous distribution of the deformation. Most importantly, from table 3, these local misorientations are lower in some twinned

parts (T1-T2, T6-T7) than in their parent grains (G1-G2, G12). Thus it is shown experimentally for the first time that the twinning process is associated to a further decrease in the stored energy during recrystallization. This can explain why the migration of old GBs happened when the recovery of the parent grains was not finished and the twins are formed during this migration.

In the following, the respective role of interfacial energy and stored energy on twinning is discussed.

Both growth accident [1], GB dissociation and nucleation of twins by stacking fault emission [4] theories involve a global decrease in the interfacial energy ΔEG . This applies for special cases where the newly created GB has a low energy [4]. In the general case, the decrease in the deformation level (stored energy) ΔES should be also considered. Therefore, the variation of total energy ΔE during twinning is described by Eq. 1, and the criterion of twinning formation is $\Delta E < 0$.

$$\Delta E = \Delta EG + \Delta ES \quad (1)$$

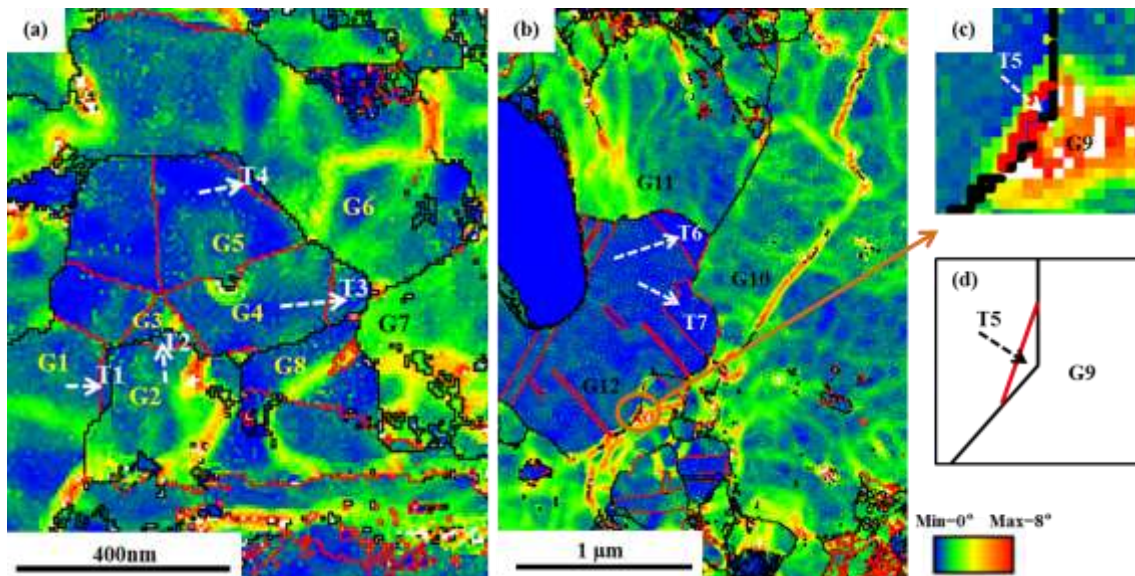


Fig. 8 (a) KAM map of Fig. 5a, and (b) KAM map of Fig. 7a. All the pixels are color coded to show the local misorientation (black and red lines show respectively the HAGBs and $\Sigma 3$ GBs). The region circled in orange in (b) is enlarged in (c) and simplified in (d)

Table 3 Average KAM values for some twin parts and grains presented in figures 8 (the value of T5

is not calculated, because it corresponds to a very small area)

Twin	Average KAM (°)	StD (°)	Growing			Shrinking grain	Average KAM (°)	StD (°)
			grain (Parent grain)	Average KAM (°)	StD (°)			
T1	0.7	0.4	G1	1.2	1.1	G2	1.8	1.5
T2	0.6	0.4	G2	1.8	1.5	G3	1.2	1.7
T3	0.6	0.3	G4	0.8	0.5	G6	1.3	0.8
						G7	2.6	1.2
						G8	0.9	0.9
T4	0.6	0.3	G5	0.5	0.4	G6	1.3	0.8
T5	/	/	G12	0.5	0.5	G9	2.9	2.1
T6	0.1	0.1	G12	0.5	0.5	G11	1.5	0.9
T7	0.2	0.2	G12	0.5	0.5	G10	1.3	0.6

1 In the example shown in Fig. 5e, the GB 30 and $\langle 111 \rangle$ is 1.5%. If the GB plane is
2 AB has migrated and a twin boundary AA' is 31 restrained to $\{100\}$ and $\{111\}$ planes
3 formed. The variation in interfacial energy due 32 respectively, the proportion of such twist GBs
4 to the twin formation is written as equation (2). 33 is negligible. For most other high angle GBs,
5 34 the energy varies from 1 to 1.4 J/m².
6 $\Delta EG = (\gamma_{AA'} \times S_{AA'} + \gamma_{A'B} \times S_{A'B}) - \gamma_{AB} \times S_{AB}$ (2) 35
7 36 Thus it can be assumed that the variation
8 Where S is the GB surface and γ is the 37 of grain boundary energy ΔEG during twinning
9 interfacial energy. The grain boundary energy 38 is almost negligible. Then ΔE includes only the
10 $\gamma_{AA'}$ for coherent twin is almost zero. Moreover, 39 variation of stored energy before and after
11 at the onset of twinning, the surface of newly 40 twinning, ΔES (Eqs. 3 and 4):
12 formed interface A'B is almost equal to that of 41 $\Delta ES = [\Delta G_{SA} \times V_A + \Delta G_{SA'} \times V_{A'} + \Delta G_{SB}$
13 AB. Also GBs AB and A'B are high angle GBs 42 $(V_B - V_{A'})] - (\Delta G_{SA} \times V_A + \Delta G_{SB} \times V_B)$ (3)
14 with 57° and 19° misorientation. Even though 43
15 the grain boundary energy depends on its 44
16 structure, it is always considered as high and 45
17 similar for all high angle GBs (misorientation 46
18 angle greater than 15°, including $\Sigma 9$) except for 47
19 the $\Sigma 3$ and $\Sigma 11$ $\{113\}$ symmetrical ones [5-6, 48
20 21, 36-37]. Energy computation of a large set 49
21 of GBs confirm the low energy of these GBs 50
22 and those vicinal to these orientations [38]. 51
23 Twist $\langle 111 \rangle$ GBs and in a less extent twist 52
24 $\langle 100 \rangle$ GBs also display a low energy. Using an 53
25 approach that determines the geometrical 54
26 probabilities for finding GBs lying close to 55
27 specific orientations in a polycrystalline 56
28 aggregate [39], the proportion of GBs with a 57
29 misorientation axis deviated by 2° from $\langle 100 \rangle$ 58 considered as zones with non-null stored

1 energy (G1 and G2 in Fig. 8a).

2 In the absence of recovery, which should
3 decrease rapidly the stored energy, the ΔG_{SB}
4 value for the deformed area depends on the
5 strain amount ε prior to heat treatment (Eq. 5).
6 C is a constant.

$$\Delta G_{SB} = - C \times \varepsilon \times V_A \quad (5)$$

7
8 As the twin area corresponds to a well
9 recrystallized area, the energy variation ΔE
10 reduces to ΔG_{SB} . In summary, a higher strain
11 before annealing leads to a higher decrease in
12 stored energy by twinning, and this favors twin
13 formation. This hypothesis is in agreement with
14 statistical results of Fig. 6. The influence of
15 stored energy or prior deformation on twin
16 formation is emphasized by the Fig. 9 that
17 shows the number of twin boundaries per grain
18 as a function of grain size, after complete
19 recrystallization of sample A [16]. Before the
20 recrystallization treatments, this sample was
21 deformed up to different strain levels. The
22 number of twin boundaries increases with the
23 grain size as expected. It is worth noting that
24 for a given grain size, a higher prior
25 deformation induces a higher number of twins
26 formed at the onset of recrystallization.

28 4.3 Mechanism of annealing twins

29 The mechanism of twinning is still
30 controversial. Depending on the authors, it
31 could result from a growth accident or be
32 produced by emission of partial dislocations
33 from the migrating GBs.

34 The annealing twins can be easily
35 developed by higher strain amount that favors
36 the higher velocity of GB migration during
37 annealing. Conversely, it was also found that
38 twin formation happened to restart the
39 restrained grain growth or GB migration,
40 during annealing at low temperature [13].
41 Twinning is an accommodation mechanism that
42 favors the dislocation slip and GB migration to
43 induce stress relaxation. During migration in
44 the deformed matrix, GBs absorb lattice

45 dislocations that give rise to a non-equilibrium
46 state. For higher migration rate, more
47 dislocations will be absorbed, and their
48 accommodation in the GB will be more
49 difficult. These arguments, associated with the
50 occurrence in the present partially
51 recrystallized nickel alloys of microtwins with
52 partial dislocations support the role of emission
53 of partial dislocations from moving GBs.
54 Moreover, this mechanism has been shown to
55 occur in MD simulations [10].

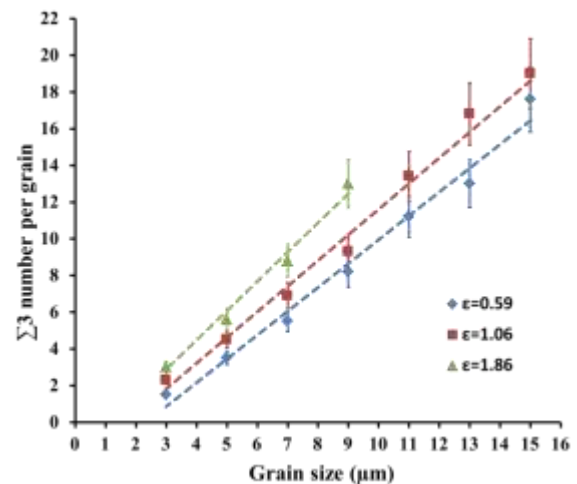


Fig. 9 Number of twin boundaries (including $\Sigma 3_{\text{coh}}$ and $\Sigma 3_{\text{incoh}}$ ones) as a function of grain size after complete recrystallization of sample A. The three curves correspond to three different strain levels, 0.59, 1.06 and 1.86 undergone by the sample before annealing treatments

5 Conclusions

It is concluded that twinning depends on the stored energy that is typically the driving force for nucleation and grain growth during the primary recrystallization. A higher stored energy gradient favors the twin formation because of the higher GB migration rate. Moreover, the presence of second phase allows the local deformation around the particles that increases locally the GB migration. This favors also the twin formation.

As a matter of fact, a decrease in stored

1 energy in twinned parts is directly emphasized
2 from local misorientation measurements in the
3 present experiments. Additionally, twinning
4 plane is related to the direction of GB
5 migration or grain growth, whatever the
6 recrystallization mechanism (SIBM or PSN).
7 When one of the 4 $\langle 111 \rangle$ axes of a grain is
8 very close to its growth direction, a coherent
9 twin is formed with this axis as the common
10 axis. This condition explains the twin
11 orientation selection among the four possible
12 variants.

14 Acknowledgement

15 The authors wish to thank Isabelle
16 DROUELLE, Denis SOLAS and Thierry
17 AUGER for fruitful discussions, and
18 acknowledge the support of Aubert & Duval for
19 providing the material.

21 References

22 [1] Fullman RL and Fisher JC (1951)
23 Formation of annealing twins during grain
24 growth, *J Appl Phys* 22: 1350-1355.
25 [2] Ashby MF and Harper E (1967) Harvard
26 Rept. Sept, Harvard University, Cambridge,
27 MA.
28 [3] Gleiter H (1969) The formation of
29 annealing twins, *Acta Metall* 17: 1421-1428.
30 [4] Meyers MA and Murr LE (1978) A model
31 for the formation of annealing twins in fcc
32 metals and alloys, *Acta Metall* 26: 951-962.
33 [5] Sutton AP, Balluffi RW (1995) *Interfaces in*
34 *Crystalline Materials*. Clarendon Press, Oxford.
35 [6] Priester L (2013) *Grain Boundaries: From*
36 *Theory to Engineering*. Springer, Dordrecht.
37 [7] Mahajan S, Pande CS, Imam MA, Rath
38 BB(1997) Formation of annealing twins in fcc
39 crystals, *Acta Mater* 45: 2633-2638.
40 [8] Rath BB, Imam MA, Pande CS (2000)
41 Nucleation and growth of twin interfaces in fcc
42 metals and alloys, *Mater. Phys. Mech* 1: 61-66.
43 [9] Dash S, Brown N (1963) An investigation

of the origin and growth of annealing twins,
Acta Metall 11: 1067-1075.

[10] Farkas D, Bringa E, Caro A (2007)
Annealing twins in nanocrystalline fcc metals:
A molecular dynamics simulation, *Phys. Rev. B*
75: 184111 (1-5).

[11] Huang P, Dai GQ, Wang F, Xu KW, Li YH
(2009) Fivefold annealing twin in
nanocrystalline Cu, *Appl. Phys. Lett* 95:
203101 (1-3).

[12] Pande CS, Imam MA, Rath BB (1990)
Study of annealing twins in fcc metals and
alloys, *Metal. Trans A* 21: 2891-2896.

[13] Field DP, Bradford LT, Nowell MM, Lillo
TM (2007) The role of annealing twins during
recrystallization of Cu, *Acta Mater* 55:
4233-4241.

[14] Bair JL, Hatch SL, Field DP (2014)
Formation of annealing twin boundaries in
nickel, *Scripta Mater* 81: 52-55.

[15] Jones AR (1981) Annealing twinning and
the nucleation of recrystallization at grain
boundaries, *J. Mater. Sci* 16: 1374-1380.

[16] Wang W, Brisset F, Helbert AL, Solas D,
Drouelle I, Mathon MH, Baudin T (2014)
Influence of stored energy on twin formation
during primary recrystallization, *Mat. Sci. Eng.*
A 589: 112-118.

[17] Jin Y, Bernacki M, Rohrer GS, Rollett AD,
Lin B, Bozzolo N (2013) Formation of
annealing twins during recrystallization and
grain growth in 304L austenitic stainless steel,
Mater. Sci. Forum 753: 113-116.

[18] Jin Y, Lin B, Bernacki M, Rohrer GS,
Rollett AD, Bozzolo N (2014) Annealing twin
development during recrystallization and grain
growth in pure nickel, *Mat. Sci. Eng. A* 597:
295-303.

[19] Zhao H, Weatherly GC (1990) The
formation of multi-domain precipitates in a
Ni-W alloy, *Acta Metall. Mater* 38: 2253-2260.

[20] Rauch EF, Veron M (2005) Coupled
microstructural observations and local texture
measurements with an automated

1 crystallographic orientation mapping tool 45
2 attached to a TEM, *Materialwiss. Werkstofftech* 46
3 36: 552-556. 47

4 [21] Humphreys FJ, Hatherly M (2004) 48
5 Recrystallization and related annealing
6 phenomena 2nd edn. Elsevier, Oxford. 49

7 [22] Beck PA, Sperry PR (1950) Strain induced 50
8 grain boundary migration in purity aluminum, *J* 51
9 *Appl. Phys* 21: 150-152. 52

10 [23] Penelle R, Baudin T (2010) Primary 53
11 recrystallization of Invar, Fe-36%Ni alloy: 54
12 origin and development of the cubic texture, 55
13 *Adv. Eng. Mater* 12: 1047-1052. 56

14 [24] Cahn JW, Mishin Y (2009) 57
15 Recrystallization initiated by low-temperature 58
16 grain boundary motion coupled to stress, *Int. J.* 59
17 *Mat. Res* 100: 510-515. 60

18 [25] Randle V (2004) Twinning-related grain 61
19 boundary engineering, *Acta Mater* 52: 62
20 4067-4081. 63

21 [26] Melmed AJ, Hayward DO (1959) On the 64
22 occurrence of fivefold rotational symmetry in 65
23 metal whiskers, *J Chem Phys* 31: 545-546. 66

24 [27] Marks LD (1994) Experimental studies of 67
25 small particle structures, *Rep. Prog. Phys* 57: 68
26 603-649. 69

27 [28] An XH, Lin QY, Wu SD, Zhang ZF, 70
28 Figueiredo RB, Gao N, Langdon TG (2011) 71
29 Formation of fivefold deformation twins in an 72
30 ultrafine-grained copper alloy processed by 73
31 high-pressure torsion, *Scripta Mater* 64: 74
32 249-252. 75

33 [29] Hofmeister H (2004) Fivefold twined 76
34 nanoparticles. In: Nalwa HS (eds) 77
35 *Encyclopedia of Nanoscience and* 78
36 *Nanotechnology* 3th volume. American 79
37 Scientific Publishers, California, pp.431-452. 80

38 [30] Bringa EM, Farkas D, Caro A, Wang YM, 81
39 McNaney J, Smith R (2008) Fivefold twin 82
40 formation during annealing of nanocrystalline 83
41 Cu, *Scripta Mater* 59: 1267-1270. 84

42 [31] Zhu YT, Liao XZ, Valiev RZ (2005) 85
43 Formation mechanism of fivefold deformation
44 twins in nanocrystalline face-centred-cubic
metals, *Appl. Phys. Lett* 86: 103112 (1-3).

[32] Bozzolo N, Souaï N, Logé RE (2012)
Evolution of microstructure and twin density
during thermomechanical processing in a γ - γ'
nickel-based superalloy, *Acta Mater* 60:
5056-5066.

[33] Wright SI, Larsen RJ (2002) Extracting
twins from orientation imaging microscopy
scan data, *J Microsc* 205: 245-252.

[34] Brewer LN, Field DP, Merriman CC (2009)
Mapping and assessing plastic deformation
using EBSD. In: Schwartz AJ, Kumar M,
Adams BL, Field DP (eds) *Electron*
Backscatter Diffraction in Materials Science
2nd edn. Springer, New York, 2009,
pp.251-262.

[35] Calcagnotto M, Ponge D, Demir E, Raabe
D (2010) Orientation gradients and
geometrically necessary dislocations in
ultrafine grained dual-phase steels studied by
2D and 3D EBSD, *Mat. Sci. Eng. A* 527:
2738-2746.

[36] Volovitch P, Baudin T, Penelle R, Caleyo F,
Barrallier L (2007) Role of recovery in the
recrystallization simulation application to a
cold rolled IF-Ti steel and a cold drawn copper
wire, *Mater. Sci. Forum* 550: 453-458.

[37] Duparc OH, Couzinié JP,
Thibault-Pénisson J, Lartigue-Korinek S,
Décamps B, Priester L (2007) Atomic
structures of symmetrical and asymmetrical
facets in a near $\Sigma=9\{221\}$ tilt grain boundary in
copper, *Acta Mater* 55: 1791-1800.

[38] Olmsted DL, Foiles SM, Holm EA (2009)
Survey of computed grain boundary properties
in face-centered cubic metals: I. Grain
boundary energy, *Acta Mater* 57: 3694-3703.

[39] Warrington DH, Boon M (1975) Ordered
structures in random grain boundaries; some
geometrical probabilities, *Acta Metall* 23:
599-607.